Scattering-aware Holographic PIV with Physics-based Motion Priors Supplement

Miao Qi, Ni Chen and Wolfgang Heidrich, *IEEE Fellow*

1 Fourier Beam Propagation Method

In this section, we provide a comprehensive derivation to support the use of the multi-slice beam propagation method. We assume that

$$\nabla_{\perp}^2 = \frac{\partial^2}{\partial x^2} + \frac{\partial^2}{\partial y^2} \tag{1}$$

Get second derivative for main paper Eq. 4 with respect to z:

$$\frac{\partial^2 u(\mathbf{r})}{\partial z^2} = \exp(jk_0 n_0 z)(\frac{\partial^2 a(\mathbf{r})}{\partial z^2} + 2jk_0 n_0 \frac{\partial a(\mathbf{r})}{\partial z} - k_0^2 n_0^2 a(\mathbf{r})) \tag{2}$$

Substitute Eq. 2 to the main paper Eq. 1 and divide the $\exp(jk_0 n_0 z)$ on both sides. We can get the following equation:

$$\frac{\partial^2 a(\mathbf{r})}{\partial z^2} + 2jk_0 n_0 \frac{\partial a(\mathbf{r})}{\partial z} + \nabla_{\perp}^2 a(\mathbf{r}) + (k_0^2 n^2 - k_0^2 n_0^2) a(\mathbf{r}) = 0 \tag{3}$$

We separate the wave amplitude into propagation direction and lateral directions:

$$a(\mathbf{r}) = a(x, y) \exp(\gamma z) \tag{4}$$

substitute the wave amplitude in Eq. 4 into Eq. 3, and divide both sides by $a(\mathbf{r})$ we have:

$$2jk_0 n_0 \gamma + \gamma^2 = \nabla_{\perp}^2 + k_0^2 (n^2 - n_0^2) \tag{5}$$

Then we get:

$$\gamma = j\{-k_0 n_0 \pm \sqrt{k_0^2 n_0^2 + (\nabla_{\perp}^2 + k_0^2 (n^2 - n_0^2))}\} \tag{6}$$

Since the wave is propagate in the $+z$ directin, we take the plus sign in Eq. 6. Now, we expand the term inside the exponential function of the Eq. 6:

$$\begin{aligned} &(k_0^2 n_0^2 + (\nabla_{\perp}^2 + k_0^2 (n^2 - n_0^2)))^{1/2} \\ &\quad = (k_0^2 n_0^2 + \nabla_{\perp}^2)^{1/2} \{1 + \frac{k_0^2 (n^2 - n_0^2)}{k_0^2 n_0^2 + \nabla_{\perp}^2}\}^{1/2} \\ &\quad = (k_0^2 n_0^2 + \nabla_{\perp}^2)^{1/2} \{1 + \frac{1}{2} \frac{k_0^2 (n^2 - n_0^2)}{k_0^2 n_0^2 + \nabla_{\perp}^2}\} \end{aligned} \tag{7}$$

- *Miao Qi and Wolfgang Heidrich are with the Visual Computing Center, King Abdullah University of Science and Technology, Thuwal 23955-6900, Saudi Arabia*
  E-mail: miao.qi@kaust.edu.sa; wolfgang.heidrich@kaust.edu.sa;
- *Ni Chen is with Wyant College of Optical Sciences, University of Arizona, Tucson, AZ 85721-0077, USA*
  E-mail: nichen@arizona.edu

$\nabla_{\perp}^2$ represents the Laplacian operator squared in the perpendicular (lateral) directions. The wave number in the lateral directions is significantly smaller than the wave number in the propagation direction. Hence, we have $\nabla_{\perp}^2 \ll k_0^2 n_0^2$. Additionally, by approximating $(n^2 - n_0^2) = (n + n_0)(n - n_0) \approx 2n_0(n - n_0)$ [1], [2], [3]. We can simplify the Eq. 7 to:

$$\begin{aligned} &(k_0^2 n_0^2 + \nabla_{\perp}^2)^{1/2} + \frac{1}{2} k_0^2 (n^2 - n_0^2)(k_0 n_0^2 + \nabla_{\perp}^2)^{-1/2} \\ &= (k_0^2 n_0^2 + \nabla_{\perp}^2)^{1/2} + k_0^2 \frac{n_0}{k_0 n_0} (n - n_0) \\ &= (k_0^2 n_0^2 + \nabla_{\perp}^2)^{1/2} + k_0 (n - n_0) \end{aligned} \tag{8}$$

substituting this into Eq. 6 and into Eq. 4:

$$a(x, y, z + \Delta z) = \exp((N + D)\Delta z) a(x, y, z) \tag{9}$$

where

$$\begin{aligned} &D = j\{\sqrt{k_0^2 n_0^2 + \nabla_{\perp}^2} - k_0 n_0\} \quad N = jk_0 \Delta n(\mathbf{r}) \\ &\Delta n(\mathbf{r}) = n(\mathbf{r}) - n_0(\mathbf{r}) \end{aligned} \tag{10}$$

We separate the Eq.9 into two parts. One D is a shift-invariant which is not related with $\Delta n(\mathbf{r})$. The other N is related with $\Delta n(\mathbf{r})$. However D and N operator are not commnute operator, therefore, there will be some error if we do expansion and write it as:

$$a(x, y, z + \Delta z) = \exp(N\Delta z) \exp(D\Delta z) a(x, y, z) \tag{11}$$

The error can be estimate by the Baker-Campbell-Hausdorff formula [4], it is related with the slice depth Δz. By change to Fourier domain, we can find that the $\nabla_{\perp}^2$ correspond to the spectrum frequency $-k_x^2 - k_y^2$ in lateral direction [1]. For D operator we can explain is as a free propagation from z to $z + \Delta z$:

$$\begin{aligned} &a(x, y, z + \Delta z) \\ &= \mathcal{F}^{-1}\{\mathcal{F}[a(x, y, z)] \times \exp(j\Delta z \sqrt{k_0^2 n_0^2 - k_x^2 - k_y^2} - k_0 n_0)\} \end{aligned} \tag{12}$$

For N operator we can explain it as phase delay:

$$a(x, y, z + \Delta z) = \exp(jk_0(\Delta n(\mathbf{r}))\Delta z) a(x, y, z) \tag{13}$$

Eq. 12 and Eq. 13 are the formulas used in the main paper Section. 3.

2 Horn-Schunck Opitcal Flow

In order to solve the Eq.(19) in main paper, we change it to the continuous model and take it as a calculus of variant problem. For every consecutive two frames, we think that $n(x, y, z, t)$ as a function of spatial and temporal coordinate x, y, z, t. Define the u, v, k as the velocity field component in x, y, z direction. We define a energy function as below:

$$E(u,v,k) = \iiint \kappa_1(n_x u + n_y v + n_z k + n_t)^2 + \kappa_2(\|\nabla u\|^2 + \|\nabla v\|^2 + \|\nabla k\|^2)\, dx\, dy\, dz \tag{14}$$

The n_x, n_y, n_z mean the derivative with respect to x, y, z coordinate. s_t mean the temporal derivative.

We want to find the minimum value of this energy function and its optimal point. Therefore, we use the Euler-Lagrange equation:

$$\begin{aligned}
\frac{\partial E}{\partial u} - \frac{\partial}{\partial x}\frac{\partial}{\partial u_x} - \frac{\partial}{\partial y}\frac{\partial}{\partial u_y} - \frac{\partial}{\partial z}\frac{\partial}{\partial u_z} = 0 \\
\frac{\partial E}{\partial v} - \frac{\partial}{\partial x}\frac{\partial}{\partial v_x} - \frac{\partial}{\partial y}\frac{\partial}{\partial v_y} - \frac{\partial}{\partial z}\frac{\partial}{\partial v_z} = 0 \\
\frac{\partial E}{\partial k} - \frac{\partial}{\partial x}\frac{\partial}{\partial k_x} - \frac{\partial}{\partial y}\frac{\partial}{\partial k_y} - \frac{\partial}{\partial z}\frac{\partial}{\partial k_z} = 0
\end{aligned} \tag{15}$$

Then we get:

$$\begin{aligned}
\kappa_1 n_x(n_x u + n_y v + n_z k + n_t) - \kappa_2 \Delta u = 0 \\
\kappa_1 n_y(n_x u + n_y v + n_z k + n_t) - \kappa_2 \Delta v = 0 \\
\kappa_1 n_z(n_x u + n_y v + n_z k + n_t) - \kappa_2 \Delta k = 0
\end{aligned} \tag{16}$$

The Δ is the Laplace operator. By solving this linear equations (16), we can get the optimal point and get the value of $\mathbf{v_t}$ for every two consecutive frames.

For the optical flow Eq. (16) we use a matrix free conjugate gradient descent algorithm to solve it.

3 Implementation Detail

For hardware setup, we use the Thorlab CPS532 laser. The wave length is 532 nm. We use the COP5-A collimation adaptor lens to enlarge the laser light. Then the light go through a ND filter to reduce the brightness. Then it will go through a collimator which is made of two singlet lenses like Fig. 1. We build a customized water tank. We 3D print the frame and place two microscope glasses in the front and back. The camera we use is the FLIR Point Grey monochrome camera(GS3-U3-50S5M). The pitch size is $3.45\mu m$ We 3D print a camera cap to block the reflection light of the camera thread and camera base and install it in the camera mount. We run our algorithm on a workstation with CPU is Intel(R) Xeon(R) Gold 6136 CPU @ 3.00GHz and GPU NVIDIA V100. For the automatic differentiation optimizer, we use the ADAM optimizer. The learning rate is 0.0001. The weight for the average gradient β is 0.99 without using the AMSGrad. For the $128 \times 128 \times 100$ volume reconstruction, the weight for volume sparsity κ_1 is 0.0001 κ_2 is 0.01 . For the $1024 \times 1024 \times 100$ reconstruction κ_1 is 0.00001 κ_2 is 0.01. We have three image scale for the pyramid optical flow reconstruction. In implementation, because our tank and volume is anisotropic in different direction. Therefore, we have different weight for sparsity for x, y direction and z direction. For x, y the sparsity weight is 0.0001, for z sparsity weight is 0.000001.

Our method is not that sensitive to the hyperparameters. For resolution $128 \times 128 \times 100$, the parameters κ_0 varying from 0.001 to 0.0001, κ_1 from 0.01 to 0.001, κ_2 from 0.001 to 0.00001 result in AAE varying from 9.13 to 16.76.

4 Experiment

4.1 AAE and EPE Discussion

The AAE and EPE are defined as:

$$AAE(\mathbf{v_g}, \mathbf{v_e}) = \arccos\left(\frac{\mathbf{v_g}\cdot\mathbf{v_e}+1}{\sqrt{(\|\mathbf{v_g}\|_2^2+1)(\|\mathbf{v_e}\|_2^2+1)}}\right) \tag{17}$$

$$EPE(\mathbf{v_g}, \mathbf{v_e}) = \|\mathbf{v_g} - \mathbf{v_e}\|_2 \tag{18}$$

where $\mathbf{v_g}$ and $\mathbf{v_e}$ are the ground-truth and estimated velocity. The average angular error (AAE) is a scale-invariant measure that accommodates both large and small velocities without amplification of the error signal. However, the AAE does not account for potential differences in the relevance of errors in regions of smooth non-zero motion versus errors in regions of zero motion. Furthermore, the AAE involves an arbitrary scaling constant of 1.0 to convert the units from pixels to degrees.

Therefore, in the mean time, we also compute the end-point error (EPE), which quantifies the Euclidean distance between the ground-truth and estimated velocities. The EPE does not suffer from the limitations of the AAE and provides a more straightforward measure of the accuracy of velocity estimates [5] .

In order to have a better comparison visualization. We plot the line profile of the reconstruct particle along the x, y, z, axis. The result is shown in Fig. 1. For Fig. 1a, we choose the line profile $y = 512$ in the YZ projection plane. w/o Flow mean our particle reconstruction method without adding the particle motion consistency in Section 4.1 in main paper. w Flow+DIV mean our method with particle motion consistency constraint and divergence free physics prior. Note that the better flow reconstruction can help also help with the particle reconstruction. From Fig.1a, we can see that the particle motion consistency constraint and divergence free prior can help with the particle reconstruction and mitigate the elongation problem. Our result is very close to the ground truth. For Fig. 1(b)(c), we choose the $x = 512$ and $y = 512$ and plot the line profile along the y axis and x axis. From Fig. 1, we can see that this method have better reconstruction in x,y direction than z direction. That's because our setup is line in the z direction. The system have better lateral resolution than the depth resolution.

4.2 Synthetic Flow

We synthesis a rotation flow with formula $\mathbf{v}(x, y, z) = -y/\sqrt{x^2+y^2+z^2}\mathbf{i} + x/\sqrt{x^2+y^2+z^2}\mathbf{j} + 0\mathbf{k}$. The $\mathbf{i}, \mathbf{j}, \mathbf{k}$ mean the v component in x, y, z direction. Then doing the same forward simulation like in main paper section 5.1.1. Then we generate t_1 frame synthetic hologram. Then we warp the particle by this rotation flow. And do the same forward simulation. We get the t_2 frame synthetic hologram. To closely replicate real-world scattering results, we divided

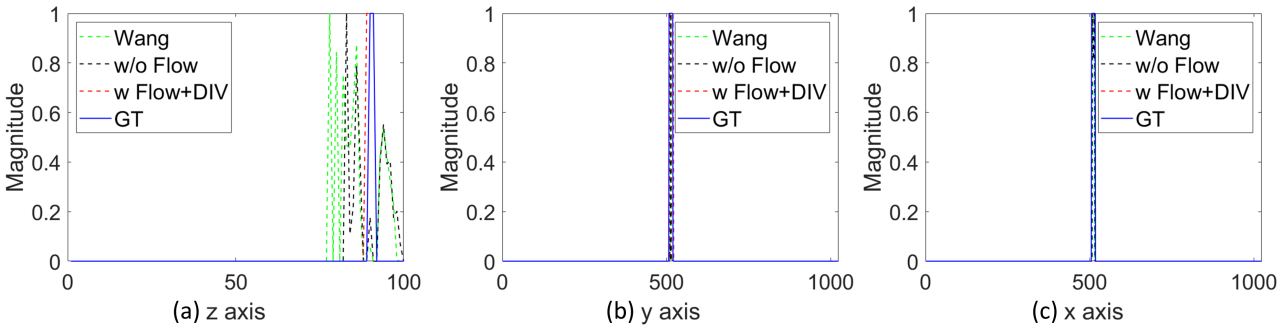

Fig. 1. The Particle Reconstruction Result Comparison. (a) is the line profile of reconstructed particle among the z axis. (b) is the line profile of reconstructed particle among the y axis.(c) is the line profile of reconstructed particle among the x axis.

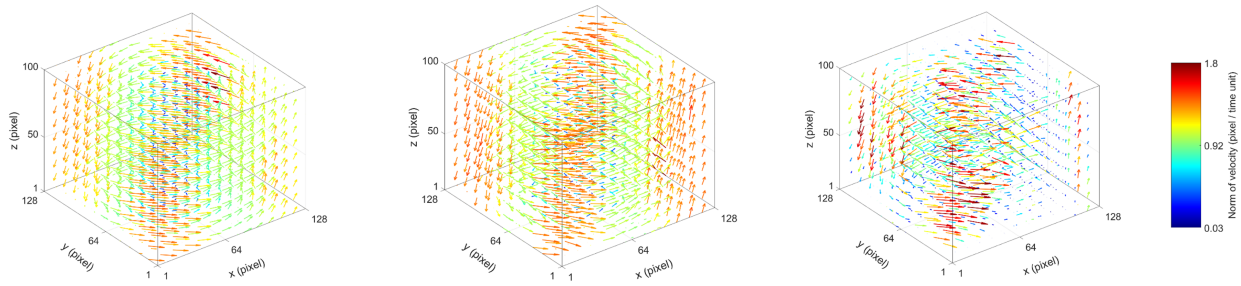

Fig. 2. The rotation flow reconstruction result. (a)Our reconstructed flow result (b) Ground truth flow (c) Flow reconstructed by Wang method

the entire volume into $1024 \times 1024 \times 10000$ voxels for the forward simulation of the hologram. The reconstruction voxel number is $1024 \times 1024 \times 100$.

Then we take these holograms as our captured images and run our reconstruction algorithm. The reconstruction voxel number is $128 \times 128 \times 100$ with scale of $1.38\mu m \times 1.38\mu m \times 30\mu m$ for every voxel. The wavelength is $632nm$. Fig. 2a is our reconstruction result. Fig. 2c is the reconstruction result by using the the Wang's method [6]. For using this method reconstruction, we do reconstruction for every hologram independently. Then compute the optical flow based on the reconstructed volume. The flow ground truth is in Fig. 2 b. We can see that our reconstruction result is very close to the ground truth and have better peformance than Wang's method. The AAE is about 12.67 and EPE is about 0.2749. While for the Wang's method, AAE is 23.68 and EPE is 1.0355.

4.3 Ablation Study

4.3.1 Different Prior Improvment Ablation Study

In order to see how our each prior affect the flow reconstruction performance, we also did a ablation study. The result is shown in Fig.3. The w/o Flow & DIV mean our particle reconstruction without adding the particle motion consistency and flow reconstruction without adding divergence free term. The w/o DIV mean that our particle reconstruction method with particle motion consistency but flow reconstruction without divergence free term. w Flow + DIV mean that our particle reconstruction method with particle motion consistency and our flow reconstruction with divergence free term. We can see the particle motion consistency help the most. This because if we have better particle reconstruction, the flow can be reconstructed more accurate. The divergence also help to improve the reconstruction result by constrain it to be divergence free and decrease more uncertainty.

4.3.2 Plane2Plane and OnePlane2Last Model

We also compute the AAE for the two models. It is shown in Fig. 4. We can see that because plane-to-plane model have better value for AAE for different particle density. As the particle density increasing, the AAE will getting worse and worse. We can see that there is a little decrease for the Plane2Plane model. That's because as particle density increasing, the more flow detail can be recovered.

4.4 Real Experiment

The real experiment setup with ground is like Fig. 5 up figure. The optical axis and the translation stage axis are perpendicular to each other. To enable quantitative assessment of the flow, a tank filled with a high-viscosity liquid was constructed. So that the particle is fixed in the tank. The high viscosity liquid is made by PDMS(sylgard 184). PDMS is a low-viscosity liquid at room temperature and can be easily molded into different shapes and patterns. To create the testing liquid, particles were mixed into the PDMS. Subsequently, the mixture was placed in a vacuum chamber for degassing to ensure the absence of bubbles within the liquid. The curing agent was then added to the PDMS in a ratio of 10:1. Following a curing period of 4 days, the PDMS

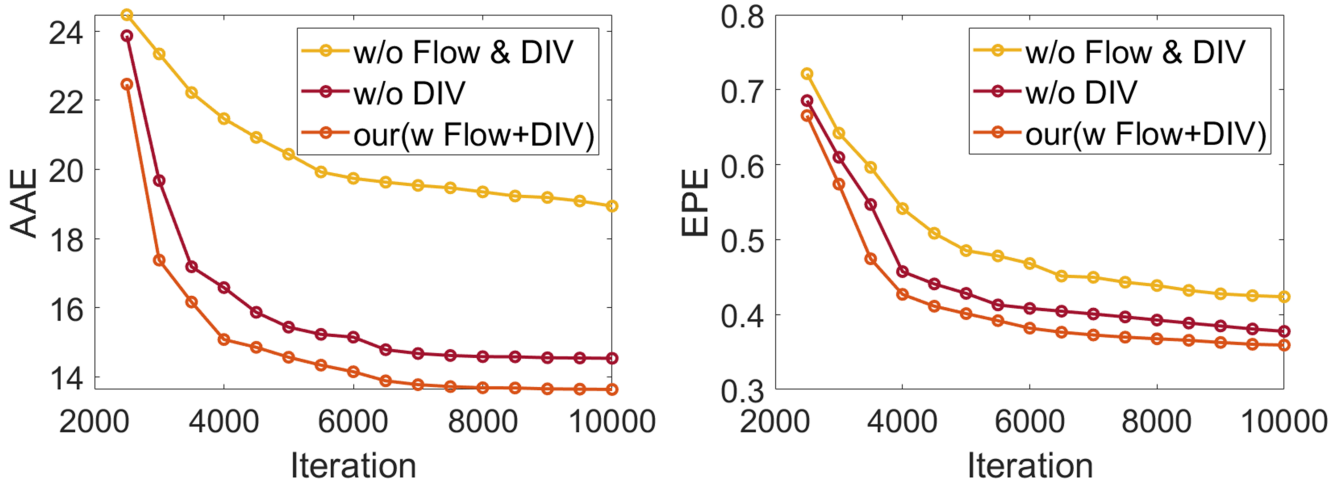

Fig. 3. The flow reconstruction result for AAE and EEP vs epoch

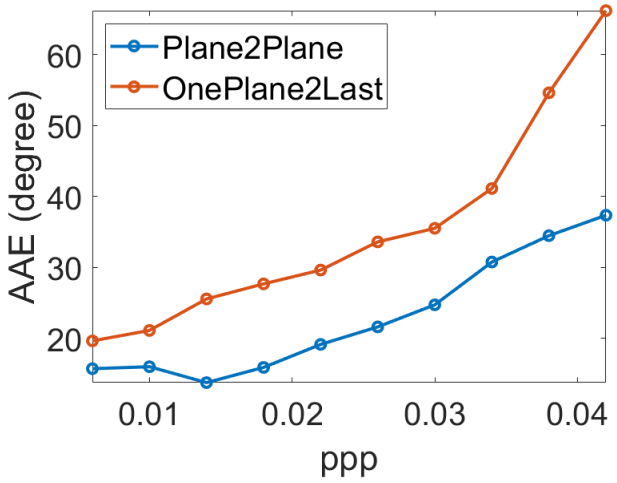

Fig. 4. The plane-to-plane model and one-plane-to-last model for different particle density.

transformed into a solid state, effectively immobilizing the particles within the material. The bottom is the translation stage figure. The right box is the motion controller. We can set the moving distance in the control software.

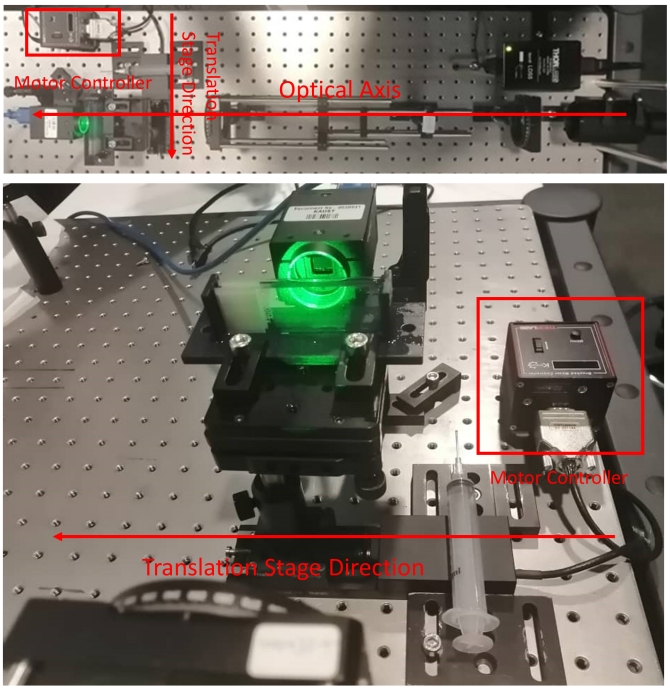

Fig. 5. Real experiment with ground truth setup. The up figure is the real experiment setup with ground truth. The bottom is the translation stage with high-viscosity ground truth tank.

REFERENCES

[1] J. W. Goodman, *Introduction to Fourier optics*. Roberts and Company publishers, 2005.

[2] M. Feit and J. Fleck, "Beam nonparaxiality, filament formation, and beam breakup in the self-focusing of optical beams," *JOSA B*, vol. 5, no. 3, pp. 633–640, 1988.

[3] K. Kawano and T. Kitoh, *Introduction to Optical Waveguide Analysis: Solving Maxwell's Equation and the Schrödinger Equation*. John Wiley & Sons, 2004.

[4] R. Gilmore, "Baker-campbell-hausdorff formulas," *Journal of Mathematical Physics*, vol. 15, no. 12, pp. 2090–2092, 1974.

[5] N. Chen, C. Wang, and W. Heidrich, "Snapshot space–time holographic 3d particle tracking velocimetry," *Laser & Photonics Reviews*, vol. 15, no. 8, p. 2100008, 2021.

[6] H. Wang, W. Tahir, J. Zhu, and L. Tian, "Large-scale holographic particle 3d imaging with the beam propagation model," *arXiv preprint arXiv:2103.05808*, 2021.